Modeling and Experimental Testing of the Hondamatic Hydro-Mechanical Transmission (HMT)

Preprint · June 2018

CITATIONS
0

READS
133

3 authors, including:

Perry Li
University of Minnesota
285 PUBLICATIONS **4,736** CITATIONS

SEE PROFILE

Modeling and Experimental Testing of the Hondamatic Hydro-Mechanical Transmission (HMT)

Xiaodong Hu, Chongbo Jing and Perry Y. Li

***Abstract*—A hydro-mechanical transmission (HMT) is a continuously variable transmission that transmits power both mechanically and hydraulically. A typical HMT consists of a pair of hydraulic pump/motors and a mechanical transmission in parallel, making it bulky and costly. The Hondamatic transmission is a compact alternative HMT design that uses an inline configuration such that the rotation of the piston barrels of the pump and motor are dual-used for mechanical transmission. This is achieved using a two-shafted pump that plays the role of a planetary gear and a distributor valve mechanism that replaces the valve plates. This paper provides the operating principle of the Hondamatic and analyzes its performance through a combination of modeling and experimentation. Specifically, ideal and lossy average models are developed, and the performance of the Hondamatic is characterized experimentally. The lossy model, fitted with seven empirically determined parameters, is capable of predicting the mechanical and volumetric losses at different ratios and operating conditions. The dominant losses are found to be compressibility losses and no-load viscous friction losses, especially on the motor side. These losses are attributed to be the main causes for the unity transmission ratio to be less efficient than expected. The overall efficiency is over 70% under most operating conditions and transmission ratios. This analytical and experimental study is the first study in the open literature on this innovative compact inline HMT configuration.**

I. Introduction

Mechanical transmissions can be configured using hydraulic machines in either a series configuration (also known as hydrostatic transmission (HST)) or a power-split configuration (also known as a hydro-mechanical transmission (HMT)). Both provide continuously variable transmission (CVT) ratios compared to conventional mechanical transmissions that only provide discrete ratios. In a HST, all power is transmitted through the pair of hydraulic pump/motors; whereas in a HMT, power is transmitted partly via the mechanical gears and partly via the hydraulic pump/motors. Since mechanical gears are typically more efficient than hydraulic pump/motors, especially when the pump/motors are at low displacements, HMT's are more efficient than HST's.

Generally, a HMT is constructed by combining a HST with a mechanical gear train in parallel. The two are coupled together with a coupling gear and at least one planetary gear set (PG). There are 4 basic HMT configurations as shown in Fig. 1 [1]: "input-coupled (coupling gear is at input and PG is at output), "output-coupled (PG is at input and coupling gear is at output), "dual stage coupled (an input-coupled with a gear-shift), and "compound (with 2 PGs). Variations of the input coupled and output coupled configurations are also provided in [2], [3]. It was shown (see e.g. [4]) that all four configurations have high efficiencies (over 80%) at all vehicle speeds, and that they are significantly more efficient than a HST, especially at part-load. Although HMTs have been known for decades, they have become more common since the introduction of several commercial products, including Fdent Vario's output coupled HMT with 2 traditional gears agricultural tractors in 1996, the S-Matic by Steyr Antriebstechnik in 2000, the c-Power by ZF Friedrichshafen's in 2001 and the "Auto Power" by John Deere. The latter three are all input-coupled compound transmissions with 4 or 5 shafts [5]. HMTs can also be hybridized by adding a hydraulic accumulator to allow for further engine management and the recuperation of braking energy. Such a hybrid hydraulic powersplit architecture combines the benefits of decoupling the engine speed from the vehicle speed (as in series architecture), and the use of mechanical gears for efficient power transmission (as in a parallel architecture) [6]. Design non-hydrid HMTs typically involve studying different arrangements and sizing of the pump/motors, gears and the location of clutches [7], [8], [9]. An efficient procedure for parameterizing and optimizing hybridized HMTs is developed in [10].

Since a HMT requires a parallel mechanical transmission in addition to a pair of hydraulic pump/motors, they tend to be heavy, bulky and expensive. An exception is the Hondamatic, a HMT developed by the Honda Motor Co.. The Hondamatic does not require a planetary gear nor a coupling gear and has an in-line configuration such that the rotation of the piston barrels of the pump/motors themselves are used for mechanical power transmission, resulting in a very compact transmission. The unit for use with an 20kW engine, is only 30 cm long with the maximum diameter of about 22cm (see Fig. 2). The Hondamatic has been deployed in some commercial All Terrain Vehicles (ATV) and motorcycles [14] since 2000.

Although the Hondamatic has been commercially available

Research performed at the Center for Compact and Efficient Fluid Power, University of Minnesota.

X. Hu is a PhD candidate at the State Key Laboratory of Fluid Power and Mechatronic Systems, Zhejiang University, Hangzhou, Zhejiang Province, 310027, P. R. China. Email: hxdtx070716@sina.com

C. Jing is with the National Key Laboratory of Vehicular Transmission, Beijing Institute of Technology, Beijing, 100081, P. R. China. Email: jingchongbo@bit.edu.cn

P. Y. Li is with the Center for Compact and Efficient Fluid Power, Department of Mechanical Engineering, University of Minnesota, 111 Church Street SE, Minneapolis, MN 55455. Email: lixxx099@umn.edu

Please send all correspondence to: Perry Li.

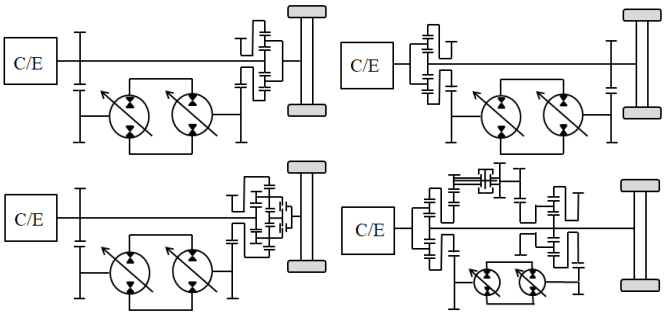

Fig. 1. Schematic of traditional HMT's. Top-left is input coupled structure, Top-right is output coupled structure, Bottom-left is dual stage coupled structure, and Bottom right is compound coupled structure.

for several years, there has been no in-depth investigation of it or of any other inline HMTs in the open academic literature. A prior inline HMT produced by Cessna is mentioned in [11]. Beyond patent description (e.g. [13], some information on its construction are provided on Honda's website [12]. It was also introduced in the PhD dissertation [15] but was simply treated as a hydro-static CVT. This paper provides both theoretic and experimental analysis of this compact HMT. It is the first such investigation in the open academic literature, as far as the authors are aware. Specifically, the operating principle of the Hondamatic is described and analyzed. Average models of the Hondamatic for both the ideal and the lossy situations are derived. Because of the interaction of the components, how the component level mechanical and volumetric losses affect the overall performance is not obvious a-priori. Whereas the volumetric losses is expectedly found to be the sum of the volumetric losses of the pump and the motor, the mechanical losses are, interestingly, revealed to be a convex combination of the pump and motor losses. The Hondamatic was also experimentally tested to evaluate its performance. The experimental results are used to obtain seven empirical parameters that describe the volumetric and mechanical losses and then the complete operation of the transmission. With the help of the lossy average models, the dominant loss mechanisms can be discovered. For example, it is found that in the specific unit tested, pressure independent viscous friction and compressibility loss on the motor side are dominant in the 1:1 mechanical lock-up ratio.

The rest of the paper is organized as follows. Section II describes the construction and operating principle of the Hondamatic. The ideal and lossy average models are presented in Section III. Section IV presents the results of the experimental testing and empirical model of the losses. Sections V and VI contain discussion and concluding remarks.

II. Structure and Operating Principle

A. Construction

The schematic of the Hondamatic is shown in Fig. 2. It consists of a 7 piston fixed displacement axial piston pump and a 9 piston variable displacement axial piston motor in opposite orientations. The piston barrels of the pump and of the motor, and the output shaft are connected mechanically. The pump and the motor are connected hydraulically via two distribution valve blocks.

Unlike a conventional axial piston pump that has a stationary casing and an input shaft connected to the piston barrel, the hydraulic pump of the Hondamatic has two mechanical ports and a casing that can be rotated. One mechanical port is the input shaft that rotates the casing via an external gear bolted to the outer circumference of the casing. The other mechanical port is the rotation of the piston barrel. The pump's pistons are pushed against a shoe-plate with the spherical ends of the piston shoes contacting the small spherical indentations on the shoe-plate. The shoe-plate is supported circumferentially against the casing by an angular contact ball bearing that rotates about an axis inclined at an angle relative to the pump axis. The inclination defines the angle of a virtual swash plate and of the shoe-plate, and hence the pump displacement. Rotating the pump casing is equivalent to rotating a virtual swash plate at an angle defined by the angle of the circumferential bearing rotating with it. This in turn causes the shoe-plate to move in and out axially. For this reason, the pump is kinematically equivalent to a wobble plate pump with the pump's swash plate being rotatable axially by the input shaft (Fig. 3). This swash plate arrangement reduces friction related energy losses at the piston shoes since the relative movements between the piston shoes and the shoe plate is small and are restricted to the radial direction. The sliding friction normally between the piston shoes and the swash plate is replaced by the bearing friction between the housing and the shoe-plate. With this design, the pump is a combination of a wobble plate pump (where the piston barrel is usually stationary and the swash plate rotates) and a conventional axial piston pump (where the swash plate is usually stationary and the piston barrel rotates). By allowing both the piston barrel and the equivalent wobble plate to rotate independently, the pump flow becomes proportional to the relative speed between the equivalent wobble plate (driven by the input shaft) and the piston barrel (driving the output shaft). The symbol on the left side of Fig. 3-bottom is used to represent the 2-shafted pump.

The hydraulic motor is a variable displacement motor that uses a similar swash plate arrangement as in the hydraulic pump. The difference is that the motor casing (or the virtual swash plate) does not rotate but it can pivot about an axis perpendicular to the motor axis to vary the swash plate angle and hence the motor displacement. The flow rate consumed by the motor is proportional to the rotational speed of the piston barrel (or the output shaft).

The pump and the motor communicate hydraulically via a distributor valve mechanism (Fig. 4), instead of the conventional valve plates. The mechanism directs flows between the pump/motor piston chambers and an outer high pressure ring or the inner low pressure chamber. Each of the pump and motor has a distribution valve block that is rigidly connected to the respective piston barrel. The two valve blocks are clamped together mechanically and communicate hydraulically via the common high pressure ring and the common low pressure chamber. Each distribution valve block has a set of spool valves. Each valve directs the flow of a pump/motor piston to

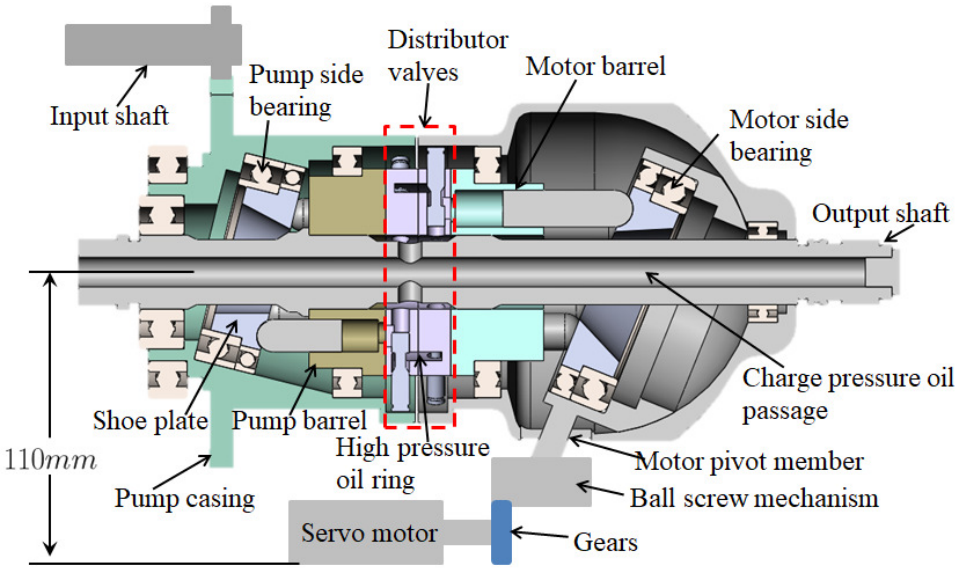

Fig. 2. Structural schematic of the Hondamatic.

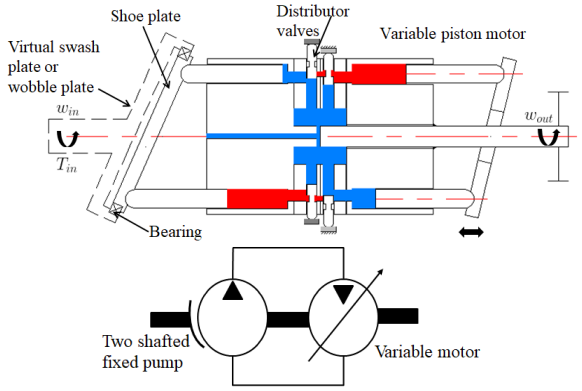

Fig. 3. A kinematically equivalent configuration of the Hondamatic.

the high pressure ring or the low pressure chamber. The spools are pushed by the pressure in the low pressure chamber against a cam ring fixed inside the corresponding pump/motor casing that is eccentrically located relative to the piston barrel. Thus, as the piston barrel rotates relative to the casing (recall that the pump casing can rotate but the motor casing is stationary), the piston chamber is connected alternately to the high pressure ring or the low pressure chamber (see Fig. 4-bottom). The eccentricity of the cam ring is designed such that for the pump, the piston chambers with decreasing volume are connected to the high pressure ring whereas the chambers with increasing volume are connected to the low pressure chamber. The reverse is true for the motor. The distributor valve design eliminates friction losses in the conventional valve plates and also has the potential of reducing leakage losses.

The pressure in the low pressure chamber is regulated externally via a small hole and a small passage through the center of the output shaft to an external charge circuit.

III. Ideal and Lossy Average Models

A. Ideal average model

The structural description above suggests that the Hondamatic functions as in the simplified diagram in Fig. 3. Here, the special pump symbol denotes a two shafted pump whose pumping function corresponds to the relative speed between the two shafts. For simplicity, we assume that the input shaft rotates the casing with a 1:1 ratio. This is equivalent to using the wobble plate pump interpretation of the Hondamatic pump in Fig. 3.

Ignoring mechanical and volumetric losses for the moment, the average model of the Hondamatic can be obtained according to the function of the individual components and their interconnections as follow:

Two-shafted pump:

$$Q_p = \frac{D_p}{2\pi}\,(\omega_{in} - \omega_{out}) \tag{1}$$

$$T_{in} = T_{me} = \frac{D_p}{2\pi}(P_H - P_T) \tag{2}$$

Motor:

$$Q_m = \frac{D_m(t)}{2\pi}\,\omega_{out} \tag{3}$$

$$J\,\dot{\omega}_{out} = T_{me} - T_{Load} + \frac{D_m(t)}{2\pi}(P_H - P_T) \tag{4}$$

where D_p and $D_m(t)$ are the fixed and variable displacements of the pump and the motor respectively, Q_p and Q_m are the flow from the pump and the flow into the motor, T_{me} is the torque applied by the pump barrel on the motor barrel, T_{in} and T_{Load} are the input torque and load torque on the output shaft, J is the combined inertia of the piston barrels and of the output shaft (lumped on the motor side).

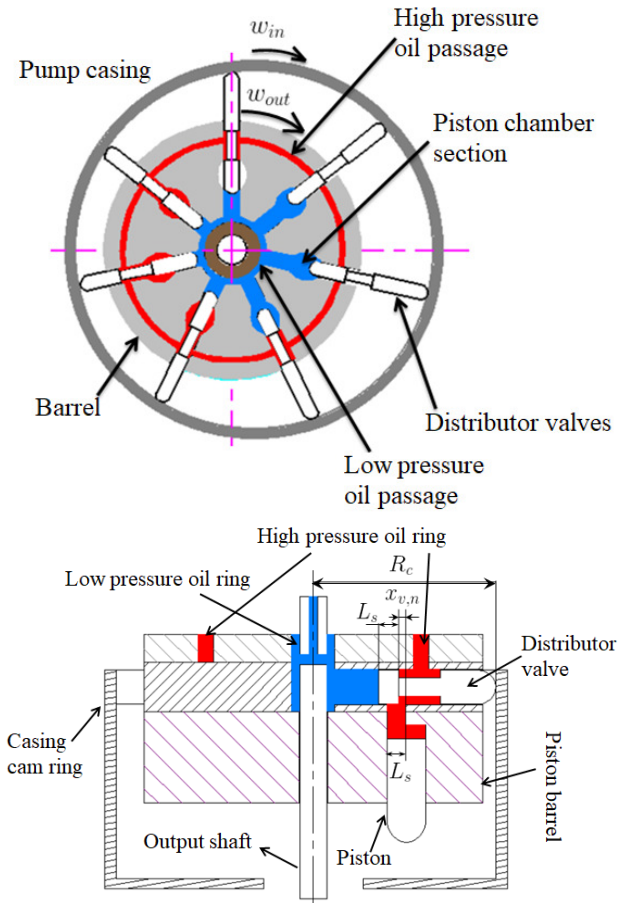

Fig. 4. Schematic of the pump side distributor valve block (top) and a detailed view of one of the valves when it is connected to high pressure (bottom). The motor side distributor valve block is similar. Each valve corresponds to one piston. The larger diameter holes in the valve bores are connected to the piston chambers. They are colored red when connected to high pressure and blue when connected to low pressure.

Combining these with the pressure dynamics of the fluid in the high pressure ring, we have:

$$\dot{P}_H = \frac{\beta}{V_{ring}}\left[\frac{D_p}{2\pi}\omega_{in} - \frac{D_p + D_m(t)}{2\pi}\omega_{out}\right] \tag{5}$$

$$J\,\dot{\omega}_{out} = \frac{D_p + D_m(t)}{2\pi}(P_H - P_T) - T_{load} \tag{6}$$

$$T_{in} = \frac{D_p}{2\pi}(P_H - P_T) \tag{7}$$

where V_{ring} is the volume of the high pressure ring and β is the bulk modulus of the fluid.

At steady state, $Q_m = Q_p$, $\dot{P}_H = 0$ and $\dot{\omega}_{out} = 0$,

$$\omega_{out} = \frac{D_p}{D_p + D_m(t)}\omega_{in} \tag{8}$$

$$T_{in} = \frac{D_p}{D_p + D_m(t)}T_{Load} \tag{9}$$

so that the input to output speed ratio or output to input torque ratio is

$$i_{ideal} = \frac{D_p + D_m(t)}{D_p}. \tag{10}$$

With the pump displacement estimated to be $D_p = 6$cc/rev and the range of motor displacement estimated to be $D_m(t) \in [-0.9, 18]$cc/rev, the range of ideal transmission ratio is $[0.85, 4]$.

The two-shafted pump can be thought of as a 1:1:1 planetary gear set with one of the shaft connected to a conventional single shaft hydraulic pump. Eq. (2) expresses the common torque relation of the planetary gear. This pump design is the key to avoid needing an actual planetary gear set to achieve the power split function. With this interpretation, the Hondamatic can be seen to be an *output-coupled input-split* architecture.

The proportion of power transmitted via hydraulic means can be computed as:

$$r_{hyd} := \frac{(P_H - P_T)\cdot Q_p}{T_{in}\omega_{in}} = 1 - \frac{\omega_{out}}{\omega_{in}} = \frac{i_{ideal} - 1}{i_{ideal}}$$

Similarly, the proportion of power transmitted mechanically is:

$$r_{mech} := \frac{T_{me}\omega_{out}}{T_{in}\omega_{in}} = \frac{\omega_{out}}{\omega_{in}} = \frac{1}{i_{ideal}} \tag{11}$$

Hence, all power is transmitted mechanically when the transmission ratio is 1, when $D_m(t) = 0$ and the transmission (pump housing, the pump and motor barrels and the output shaft) rotates like a simple mechanical shaft. Note that when $i_{ideal} < 1$, $r_{hyd} < 0$ which corresponds to power re-circulating within the transmission with the pump acting as a motor and the motor as a pump.

B. Average model with losses

We now consider how the average model in Section III-A should be modified to account for mechanical and volumetric losses. Mechanical losses include, for both the pump and motor:

- Friction torques associated with the bearings between the shoe-plates and the casing (T^P_{bear}, T^M_{bear});
- Friction torque associated with the rotation of the pump and motor barrels and the output shaft (T_{out});
- Torque due to friction between the distributor valve spools and the cam rings on the casings (T^P_v, T^M_v);
- Torque losses of the pump and the motor (T^P_{loss}, T^M_{loss}) which include friction at the pistons and piston shoes as well as throttling losses in the distributor valves.

The signs are defined such that T^P_{bear}, T^P_v, T^P_{loss} are positive when $(\omega_{in} - \omega_{out}) > 0$ and the nominal pump unit operates as a pump; and T_{out}, T^M_{bear}, T^M_v, T^M_{loss} are positive when $\omega_{out} > 0$ and the nominal motor unit operates as a motor.

Volumetric losses include:

- Leakage in the pump and the motor (Q^P_{loss}, Q^M_{loss});
- Fluid compressibility effects (Q^P_{comp}, Q^M_{comp}) which accounts for difference between the pump/motor rotation and fluid flow as a result of the fluid in the piston chamber being compressible.

Q^P_{loss} and Q^M_{loss} are assumed to be positive when the nominal pump and the motor units are pumping and motoring respectively. It is expected that Q^P_{comp} and Q^M_{comp} would increase with pressure and be proportional to the pump/motor speed $(\omega_{in} - \omega_{out})$ or ω_{out}, and the dead volumes in the pump/motor.

Incorporating these losses into the average pump, motor, barrel and pressure dynamics equations, we have:

$$Q_p = \left(\frac{D_p}{2\pi}(\omega_{in} - \omega_{out}) - Q^P_{comp}\right) - Q^P_{loss} \tag{12}$$

$$Q_m = \frac{D_m(t)}{2\pi}\omega_{out} + Q^M_{comp} + Q^M_{loss} \tag{13}$$

$$T_{me} = T_{in} - T^P_{bear} - T^P_v = \frac{D_p}{2\pi}(P_H - P_T) + T^P_{loss} \tag{14}$$

$$\begin{aligned} J\,\dot{\omega}_{out} &= T_{me} - T_{Load} - T_{out} + T^P_{bear} + T^P_v - T^M_v \\ &\quad + \frac{D_m(t)}{2\pi}(P_H - P_T) - T^M_{loss} - T^M_{bear} \end{aligned} \tag{15}$$

$$\dot{P}_H = \frac{\beta}{V_{ring}}\left[Q_p - Q_m\right] \tag{16}$$

Combining these, we have:

$$\begin{aligned} J\,\dot{\omega}_{out} &= \frac{D_p + D_m(t)}{2\pi}(P_H - P_T) - T_{load} - T_{out} \\ &\quad + (T^P_{loss} + T^P_{bear} + T^P_v) - (T^M_{loss} + T^M_{bear} + T^M_v) \end{aligned} \tag{17}$$

$$T_{in} = \frac{D_p}{2\pi}(P_H - P_T) + T^P_{loss} + T^P_{bear} + T^P_v \tag{18}$$

$$\begin{aligned} \dot{P}_H = \frac{\beta}{V_{ring}}\Bigg[&\frac{D_p}{2\pi}(\omega_{in} - \omega_{out}) - \frac{D_m(t)}{2\pi}\omega_{out} \\ &- Q^P_{comp} - Q^M_{comp} - Q^P_{loss} - Q^M_{loss}\Bigg] \end{aligned} \tag{19}$$

In the steady-state when $\dot{\omega}_{out} = 0$ and $\dot{P}_H = 0$,

$$\begin{aligned} \omega_{out} &= \frac{D_p}{D_p + D_m(t)}\omega_{in} \\ &\quad - \frac{2\pi(Q^P_{comp} + Q^M_{comp} + Q^P_{loss} + Q^M_{loss})}{D_p + D_m(t)} \end{aligned} \tag{20}$$

$$\begin{aligned} T_{in} &= \frac{D_p}{D_p + D_m(t)}(T_{Load} + T_{out} + T^M_{loss} + T^M_{bear} + T^M_v) \\ &\quad + \frac{D_m(t)}{D_p + D_m(t)}(T^P_{loss} + T^P_{bear} + T^P_v) \end{aligned} \tag{21}$$

Defining input speed loss to be the difference between the actual input speed and the theoretical input speed for the given output speed, we have

$$S_{loss} = \frac{2\pi(Q^P_{comp} + Q^M_{comp} + Q^P_{loss} + Q^M_{loss})}{D_p} \tag{22}$$

Defining the input torque loss to be the actual input torque and the theoretical input torque for the given output torque, we have

$$\begin{aligned} T_{loss} &= \frac{D_p}{D_p + D_m(t)}(T_{out} + T^M_{loss} + T^M_{bear} + T^M_v) \\ &\quad + \frac{D_m(t)}{D_p + D_m(t)}(T^P_{loss} + T^P_{bear} + T^P_v) \end{aligned} \tag{23}$$

From (22), compressibility and leakages combine to contribute to the input speed loss. Since leakages on both the pump and motor sides are dependent on the pressure in the high pressure ring, it will be difficult to distinguish their individual effect. From (23), we can identify the net torque losses on the pump side and on the motor and output side as:

$$T^P_{net-loss} := T^P_{loss} + T^P_{bear} + T^P_v \tag{24}$$

$$T^M_{net-loss} := T_{out} + T^M_{loss} + T^M_{bear} + T^M_v \tag{25}$$

and the total torque loss is a convex sum of these. In particular, when $D_m(t) = 0$, only the motor and output side torque loss contribute to the total torque loss.

As a validation of the losses, the total power loss given by:

$$\begin{aligned} &T_{in}\omega_{in} - T_{Load}\omega_{out} \\ &= \left(\frac{T_{Load}}{i_{ideal}} + T_{loss}\right)(i_{ideal}\omega_{out} + S_{loss}) - T_{Load}\omega_{out} \\ &= \frac{D_p T_{Load}}{D_p + D_m(t)}S_{loss} + T_{loss}\omega_{in} \end{aligned} \tag{26}$$

should equal the sum of the individual losses,

$$\begin{aligned} &T^P_{net-loss}(\omega_{in} - \omega_{out}) + T^M_{net-loss}\omega_{out} \\ &+(Q^P_{comp} + Q^M_{comp} + Q^P_{loss} + Q^M_{loss})(P_H - P_T) \end{aligned} \tag{27}$$

To see that this is the case, using (18) and (21), T_{Load} can be expressed in terms of $(P_H - P_T)$

$$\begin{aligned} \frac{D_p T_{Load}}{D_p + D_m(t)} &= \frac{D_p}{2\pi}(P_H - P_T) \\ &\quad + \frac{D_p}{D_p + D_m(t)}(T^P_{net-loss} - T^M_{net-loss}) \end{aligned}$$

and also using (20), ω_{in} can be expressed in terms of ω_{out} and $\omega_{in} - \omega_{out}$,

$$\begin{aligned} \omega_{in} &= \frac{D_p + D_m(t)}{D_p}\omega_{out} + S_{loss} \\ &= \frac{D_p + D_m(t)}{D_m}(\omega_{in} - \omega_{out}) - \frac{D_p}{D_m(t)}S_{loss} \end{aligned}$$

Then, substituting these respectively into the three terms of the following rearrangement of (26):

$$\begin{aligned} &\frac{D_p T_{Load}}{D_p + D_m(t)}S_{loss} + \frac{D_p}{D_p + D_m(t)}T^M_{net-loss}\omega_{in} \\ &\qquad + \frac{D_m(t)}{D_p + D_m(t)}T^P_{net-loss}\omega_{in} \end{aligned}$$

then, (27) can indeed be obtained as desired.

IV. Experiments

A. Experimental Setup

An experimental test-bed was constructed to test the performance of a Hondamatic HMT taken from a used vehicle (Fig. 5). The test circuit is shown in Fig. 6. A 28cc (Rexroth A-6) hydraulic motor is used as the prime mover to drive the input (i.e. the housing) of the Hondamatic via a 15:13 ratio coupling gear. However, for ease of interpreting the results, *the input torque and input speeds reported are translated as if the housing is rotated directly*. A 28cc (Sauer S-42) hydraulic pump is used as the dynamometer at the output. The prime mover and the dynamometer form a hydrostatic closed circuit. An external power supply (206 bar) is used to compensate for losses in the circuit. Two pairs of speed and torque sensors are located at the input and output sides of the Hondamatic to measure the input speed, input torque, output speed and output torque. A small (6.9 bar) charge pump is used to provide the charge oil to the Hondamatic. A manually controlled throttling valve upstream to the A-6 is used to control the amount of

the input power. The load can be controlled by adjusting the displacement of the S-42 dynamometer pump. A manual screw is used to control the motor displacement and hence the ideal transmission ratio of the Hondamatic.

B. Test conditions

Tests were conducted under no load condition with varying motor displacements, and at three ideal transmission ratios approximately of 1, 2.5 and 4.4 with varying speeds and loads. The input speed ranged from approximately 400 rpm to 1500 rpm and the input torque (translated to the housing) ranged approximately from 10Nm to 20Nm. This torque range corresponds to a maximum pressure of 20MPa in the high pressure ring. These speed and torque ranges are low compared to the nominal and maximum operating pressures of 36MPa and 60MPa; and the nominal and maximum input speeds of 3000rpm and 6500rpm. The power levels tested are below 4kW, which is also low compared to the 20kW engine that the transmission is intended for. Limitations in the ranges of torque and speed are due to the size of the prime mover and the flow capability of the external power supply.

C. Results

1) Transmission ratios: Figure 7 shows the speed ratios of the Hondamatic at the constant input speed of 1000rpm over the full range of motor displacements. The transmission ratio range of 0.67 to 4.34 is consistent with pump displacement of 6cc and motor displacement range of $[-0.9, 18]$cc according to (10).

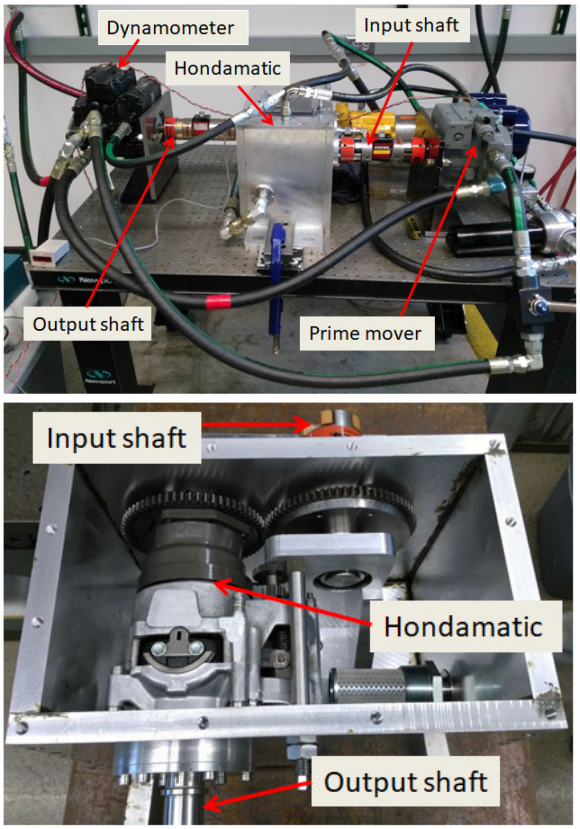

Fig. 5. Test bench(top) and the testing box that contains the Hondamatic(bottom), pictures of the test bench.

Results at the three constant displacements are presented next. The relations between the input and output speeds at different loads are shown in Fig. 8. Since deviation from the ideal ratio is due to leakage and compressibility, the ideal ratios are obtained by extrapolating the input/output speed ratios to $T_{load} = 0$ when leakage and compressibility are expected to be minimal. The three ideal ratios are found to be 0.98, 2.61 and 4.23.

In order to consider only the characteristics of the Hondamatic, the mechanical inefficiency due to the 15:13 input gear is estimated and subtracted from the input torque measurement. The torque loss due to the gear is conservatively estimated from the measured input torque with no output load. To be conservative, only the static Coulomb friction - estimated to be 0.54Nm using a procedure to be described in Section IV-C3, is removed. The actual and ideal relationships between the (adjusted) input and output torques at different loads are shown in Fig. 9.

The deviations from the ideal relationships in Figs. 8-9 are due to speed losses and torque losses respectively. These are analyzed next. The volumetric efficiency and speed loss of the Hondamatic (referred to the input) are defined as:

$$\eta_{vol} := \frac{i_{ideal}\omega_{out}}{\omega_{in}}; \quad S_{loss} := \omega_{in} - i_{ideal}\omega_{out} \tag{28}$$

where $i_{ideal}\omega_{out}$ is the ideal input speed in the absence of leakage. The mechanical efficiency and torque loss (referred to the input) are defined as:

$$\eta_{mech} := \frac{T_{load}}{i_{ideal}T_{in}}; \quad T_{loss} := T_{in} - T_{load}/i_{ideal} \tag{29}$$

2) Volumetric Efficiency: The speed losses are shown in Fig. 10-left. They indicate that speed losses increase with input torque (and therefore pressure). This is consistent with leakage generally increases with pressure. At higher torques, the speed losses also tend to increase with output speed. This dependence is consistent with fluid compressibility which introduces an apparent loss of fluid volume compared to ideal kinematic flow. Since the volume loss per rotation of the pump or the motor increases with pressure, the apparent flow loss due to fluid compressibility will be proportional to pump/motor speed and increase with pressure.

From the speed loss model in (22), assuming that leakages Q^P_{loss} and Q^M_{loss} are dependent on pressure only, and that compressibility losses Q^P_{comp} and Q^M_{comp} depend on the product of pressure, pump/motor speeds and the dead volumes, a global parameterized model of S_{loss} suitable for all ratios is:

$$\begin{aligned} S_{loss} = s_{g0}T_{in} + s_{gp}T_{in}(\omega_{in} - \omega_{out}) \\ +s_{gm}(i_{max} - i_{ideal})T_{in}\omega_{out} \end{aligned} \tag{30}$$

Here, the three terms correspond to the pressure dependent leakage, and the pump and motor side compressibility losses. The factor $i_{max} - i_{ideal}$ is used to account for the fact that the motor dead volume increases from being negligible when D_m is at maximum and $i_{ideal} = i_{max} = 4.3$ and to the

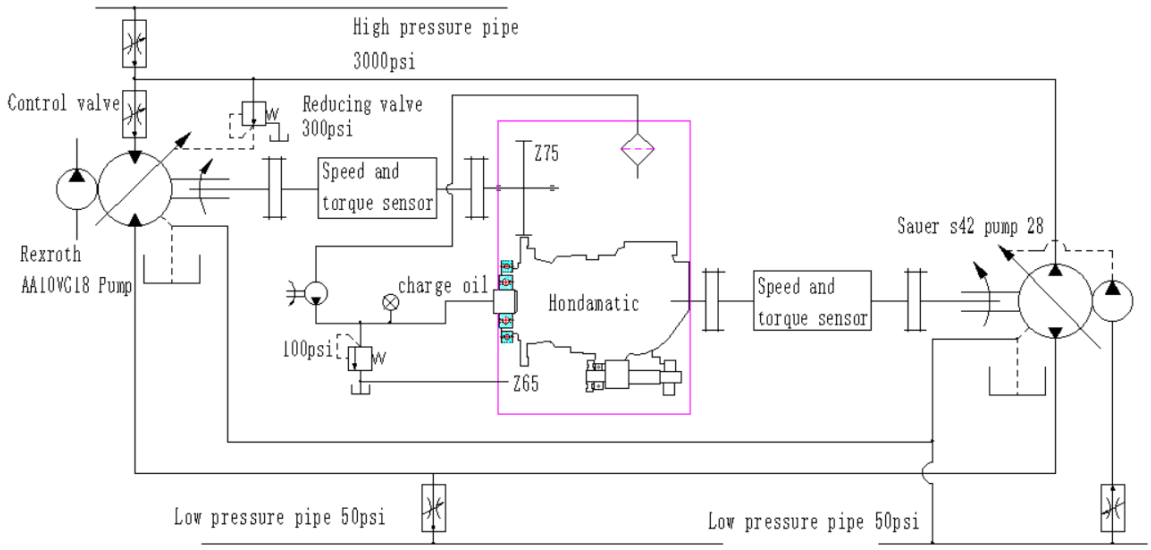

Fig. 6. The schematic diagram of the test bench.

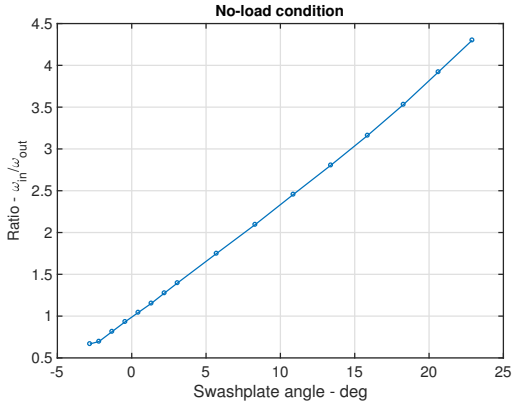

Fig. 7. Ratios between input speed and output speed when $T_{load} = 0$, $\omega_{in} \approx 1000$ rpm, and varying motor displacements.

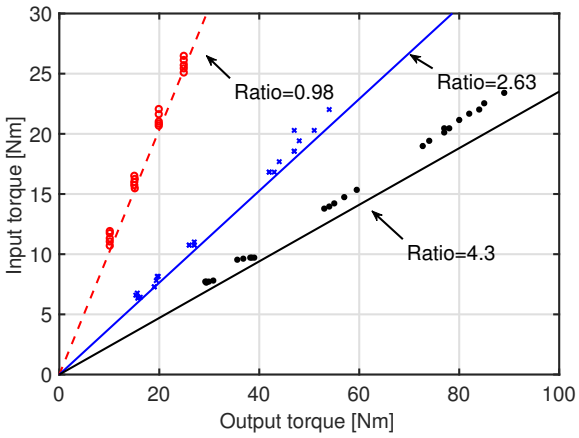

Fig. 9. Relations between input and output torques at different loads. Approximate motor swashplate angle and ideal ratios are: $(0^o, 0.98)$, $(12^o, 2.61)$; and $(22^o, 4.23)$.

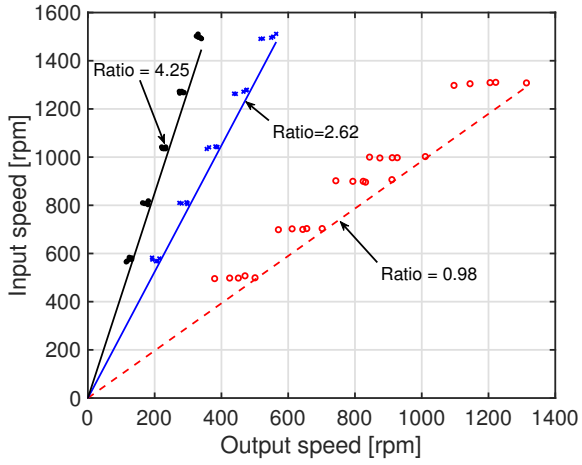

Fig. 8. Relations between input and output speeds at different loads. Approximate motor swashplate angle and ideal ratios are: $(0^o, 0.98)$, $(12^o, 2.61)$; and $(22^o, 4.23)$.

maximum when $D_m = 0$ and $i_{ideal} = 1$. A least squares fit of the data give $s_{g0} = 1.53$rpm/Nm, $s_{gp} = 0.0038$/Nm, and $s_{gm} = 0.0015$/Nm. The RMS errors at the 0deg, 12deg and 22deg motor swashplate angles are 9.6rpm, 7.9rpm and 9.9rpm respectively.

To check the validity of the model, the speed losses are modeled, for each ratio, as:

$$S_{loss} = s_0 T_{in} + s_1 T_{in} \omega_{out} \tag{31}$$

so that s_0 would correspond to s_{g0} and s_1 would correspond to $s_{g1} = s_{gp}(i_{ideal} - 1) + s_{gm}(i_{max} - i_{ideal})$ for each ratio of i_{deal}. The least squares fitted coefficients using data at each ratio and as predicted with the global model (30) are given in Table I. Note that the 3-parameter global model is able to predict the coefficients in (31) at each ratio quite well. As shown in Fig. 10-left, it is also able to fit and capture the trend of the data.

The quality of the data fit of these two sets of models are shown in Fig. 11. Both the model (31) obtained for each

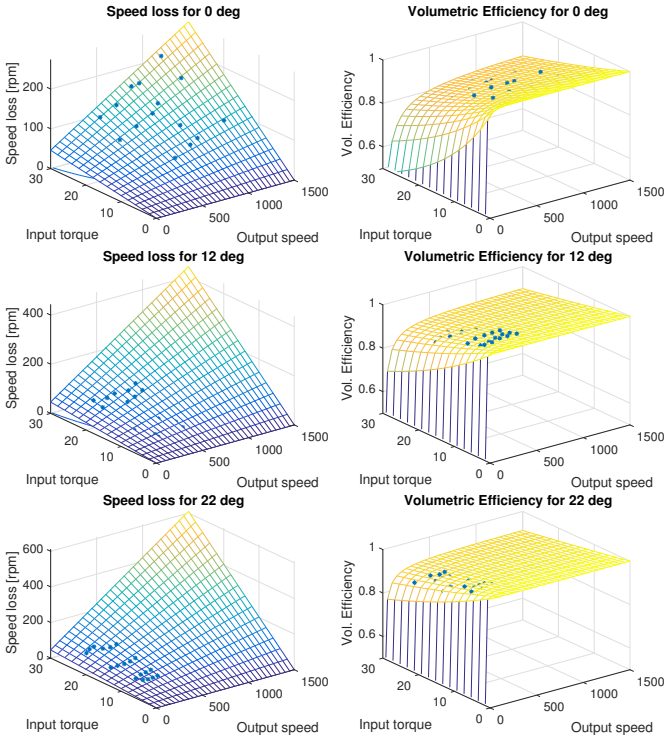

Fig. 10. Left: Input speed (volumetric) losses and their parameterization via (30). Right: Volumetric efficiencies and their parameterization via (30).Top: $i_{ideal} = 0.98$; Middle: $i_{ideal} = 2.61$; Bottom: $i_{ideal} = 4.23$. Note that some data points are close to but behind the surfaces.

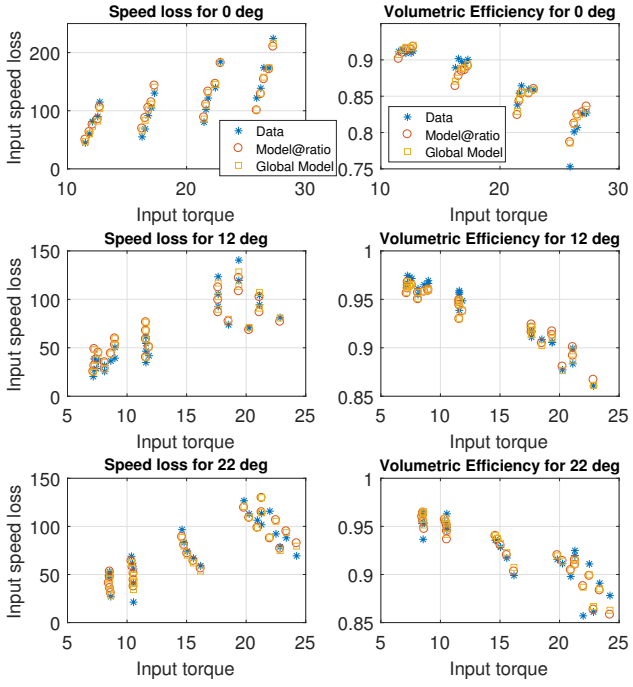

Fig. 11. Comparisons between measurements and the two models (per ratio model in (31) and global model (30)) for speed loss and volumetric efficiency at each motor swashplate angle.

TABLE I
SPEED LOSS COEFFICIENTS FOR (31) OBTAINED AT EACH RATIO AND AS PREDICTED WITH GLOBAL MODEL (30)

angle	s_0[rpm/Nm]	s_1[Nm^{-1}]	s_{g0}[rpm/Nm]	s_{g1}[Nm^{-1}]
0^o	1.9	5.3E-3	1.53	5.0E-3
12^o	1.6	9.0E-3	1.53	8.8E-3
22^o	1.9	1.3E-2	1.53	12.5E-3

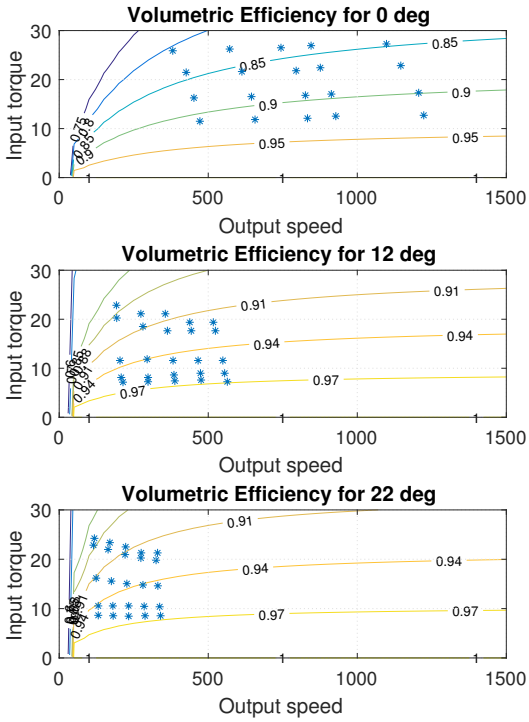

Fig. 12. Contours of volumetric efficiencies and locations of experimental data points. Top: $i_{ideal} = 0.98$; Middle: $i_{ideal} = 2.61$; Bottom: $i_{ideal} = 4.23$. Note that some data points are hidden by the surfaces.

ratio and the global model (30) provide good match to the measurement. However, the speed losses at the 0.98 ratio being highest is unexpected.

The corresponding volumetric efficiencies are shown in Figs. 10-right, 11-right and 12. The volumetric efficiencies are in the range of 75%-92% for $i_{ideal} = 0.98$, 86%-98% for $i_{ideal} = 2.61$, and 86%-97% for $i_{ideal} = 4.23$. Volumetric efficiencies decrease with input torque, as predicted. However, despite the increase in speed losses with speed, the rate of increase is gentle so that the volumetric efficiencies actually increase with speed.

3) Mechanical Efficiency: To facilitate the analysis of the torque loss and mechanical efficiency, the input torque loss is first modeled via (23) with the assumption that there exists a constant stiction at the 15:13 input gear and that $T^P_{net-loss}$ and $T^M_{net-loss}$ in (25) consist of linear viscous frictions and frictions that are proportional to the product of the pump/motor displacement and pressure. The latter assumption implies that friction between the piston and piston bore dominate. Assuming that pressure is proportional to input torque T_{in}

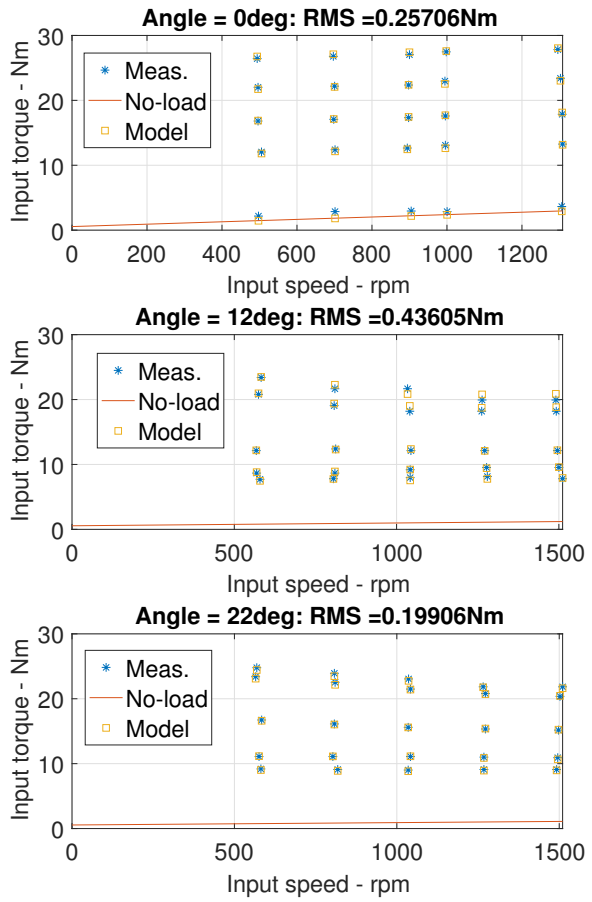

Fig. 13. Measured input torque, prediction and no-load friction according to model in (32) for the swashplate angles of 0deg, 12deg and 22deg.

and making use of (23), the form of the model is:

$$\begin{aligned} T_{loss} &= f_{st} + (1 - 1/i_{ideal})\,[b_p(\omega_{in} - \omega_{out}) + t_p T_{in}] \\ &\quad + 1/i_{ideal}\,[b_m \omega_{out} + t_m D_m/D_p T_{in}] \\ &= f_{st} + (1 - 1/i_{ideal})\,[b_p(\omega_{in} - \omega_{out}) + t_{p-m} T_{in}] \\ &\quad + 1/i_{ideal} \cdot b_m \cdot \omega_{out} \end{aligned} \tag{32}$$

where f_{st} is the stiction, b_p and b_m are the pump side and motor side viscous friction coefficients, t_p and t_m are the pump and motor side pressure dependent friction coefficients, and $t_{p-m} := t_p + t_m$, so that it is not possible to distinguish between pressure dependent frictions at the pump and at the motor. The least squares fit are shown in Fig. 13 and the parameters are found to be: $f_{st} = 0.54$Nm, $b_p = 0.46$Nm/rpm, $b_m = 1.75$Nm/rpm, and $t_{p-m} = 0.1398$Nm/Nm. The RMS error is 0.32Nm with the 2.61 ratio being the worst (0.44Nm). As mentioned earlier, the stiction is assumed to due to the 15:13 input gear and is subtracted before further analysis. It is also note worthy that the motor side viscous friction coefficient is significantly higher (nearly 4 times) than that on the pump side.

TABLE II
TORQUE LOSS COEFFICIENTS FOR EQ.(35) WITH $t_{1g} = \left(1 - \frac{1}{i_{ideal}}\right) t_{p-m}$

Angle	t_0 [Nm/rpm]	t_1 [Nm/Nm]	b_{out} [Nm/rpm]	t_{1g} [Nm/Nm]
0^o	2.1E-3	-1.47E-2	1.80E-3	-0.35E-2
12^o	1.39E-3	5.04E-2	1.18E-3	8.6E-2
22^o	1.44E-3	0.106	1.68E-3	0.106

No-load friction: The friction at no-load is extrapolated to when $T_{in} = 0$. The viscous damping coefficients referred to the input and output can be obtained by approximating $\omega_{out} \approx \omega_{in}/i_{ideal}$ as:

$$b_{in} = \left(1 - \frac{1}{i_{ideal}}\right)^2 b_p + \left(\frac{1}{i_{ideal}}\right)^2 b_m \tag{33}$$

$$b_{out} = \frac{(i_{ideal} - 1)^2}{i_{ideal}} b_p + \left(\frac{1}{i_{ideal}}\right) b_m \tag{34}$$

For $i_{ideal} \approx 1$ the damping is dominated by the motor side damping and as i_{ideal} increases, the input damping b_{in} becomes closer to that of the pump. However, since the pump side damping is significantly less than the motor side, the overall no-load damping decreases as i_{ideal} increases. b_{in} are found to be: $1.84E-3$Nm/rpm at 0deg, $0.43E-3$Nm/rpm at 12deg, and $0.36E-3$Nm/rpm at 22deg as shown in Fig. 13.

Mechanical losses with output loads: The torque losses in the presence of output loads are shown in Fig. 14-left. At $i_{ideal} = 0.98$, torque losses mainly increase with speed but with little dependence on input torque (or pressure). This suggests that the loss is dominated by viscous friction in the bearings or fluid churning, which is consistent with the fact that at this ratio, the Hondamatic rotates as a rigid body. At ratios of 2.61 and 4.23, the torque losses have strong dependence on input torque and pressure, which indicates that the various pressure dependent frictions within the transmission become more important. There is less apparent dependence on output speed, however. This is likely because at the higher ratios, the motor side friction becomes less important since $b_p << b_m$ and the motor speeds are lower.

At each ratio, the torque losses can also be modeled linearly as:

$$T_{loss} = t_0\, \omega_{out} + t_1\, T_{in} \tag{35}$$

The coefficients would be related to the globally defined model (32) via $t_0 = b_{out}$ in (34) and $t_1 = (1 - 1/i_{ideal}) t_{p-m}$. The coefficients as computed by fitting the data at each ratio and by using the global model in (32) are listed in Table II. Note that the parameters from the two methods are both similar in magnitudes and follow the same trends. The qualities of data fit using the per ratio model (35) are only slightly better than with the globally defined model (32). The latter is shown in Fig. 15.

The corresponding mechanical efficiencies are shown in Figs. 14-right. They are in the ranges of 82%-99% for $i_{ideal} = 0.98$, 79%-93% for $i_{ideal} = 2.61$, and 81%-87% for $i_{ideal} = 4.23$. The RMS error of the prediction using the global model (32) is 1.8%. At all three ratios, the mechanical efficiencies increase with input torque and decrease with

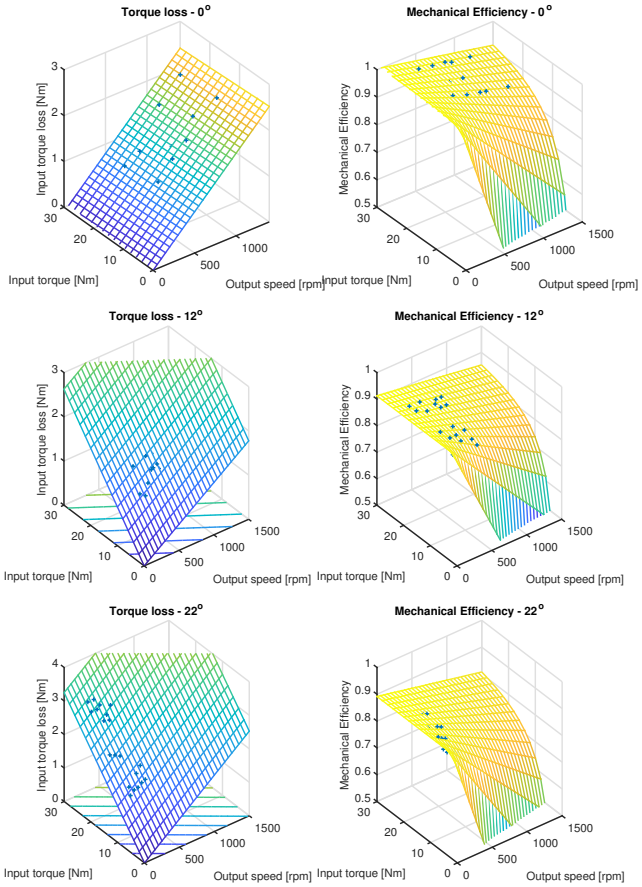

Fig. 14. Left: Input torque (mechanical) losses and their parameterization via (32). Right: Mechanical efficiencies and their parameterization via (32). Top: $i_{ideal} = 0.98$; Middle: $i_{ideal} = 2.61$; Bottom: $i_{ideal} = 4.23$. Note that some data points are hidden by the surfaces.

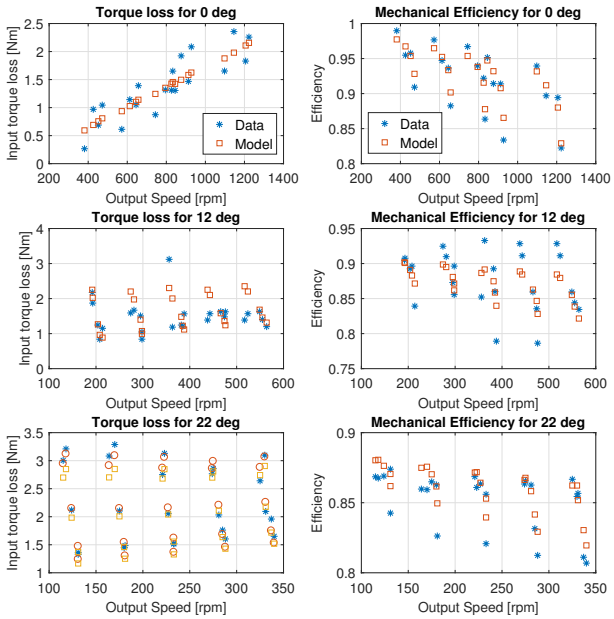

Fig. 15. Comparisons between measurements and global model (30)) for input torque loss and mechanical efficiency at each motor swashplate angle. The results from the per ratio model (35) are omitted to avoid clutter.

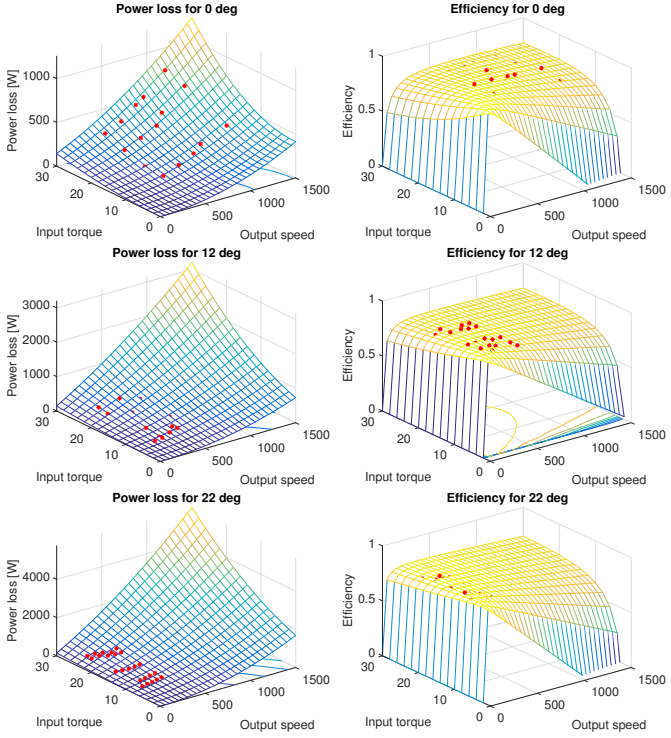

Fig. 16. Power losses and overall efficiencies. Top: $i_{ideal} = 0.98$; Middle: $i_{ideal} = 2.61$; Bottom: $i_{ideal} = 4.23$. Note that some data points are hidden by the surfaces.

output speed. Mechanical efficiency decreases with speed is due to torque loss increasing with speed. Although torque loss also increases slightly with input torque, the increase is gentle so that mechanical efficiency increases with input torque.

4) Overall Efficiency: The overall power losses and overall efficiencies are shown in Figs. 16. Models for the power losses can be constructed from models for the volumetric and mechanical losses in (31) and (35) as:

$$P_{loss} = T_{in} s_{loss}(T_{in}, \omega_{out}) + i_{ideal} \omega_{out} T_{loss}(T_{in}, \omega_{out}) \tag{36}$$

For all three ratios, the power losses increase with both output speed and input torque. The overall efficiencies are in the ranges of 75%-85% for $i_{ideal} = 0.98$, 76%-86% for $i_{ideal} = 2.61$, and 74%-84% for $i_{ideal} = 4.23$. For all three ratios, at the test cases, the overall efficiencies are fairly insensitive to both output speed and input torque.

To compare the efficiencies of the Hondamatic at different transmission ratios to transmit the same power, the efficiencies at the operating conditions tested are plotted against input power in Fig. 18. Since the experiments are done with similar input torque and input speed ranges, the ranges of power are similar for the tests performed at the three ratios. Interestingly, all three ratios have similar efficiencies within the scatter of the results. The middle ratio of 2.61 is seen to be slightly more efficient, while the ratios of 0.98 and 4.23 have similar efficiencies. In theory, the ratio of 1 should be the most efficient since all power is transmitted mechanically. However, as there is significant motor side compressibility losses and viscous friction associated with the rotation of the barrels and

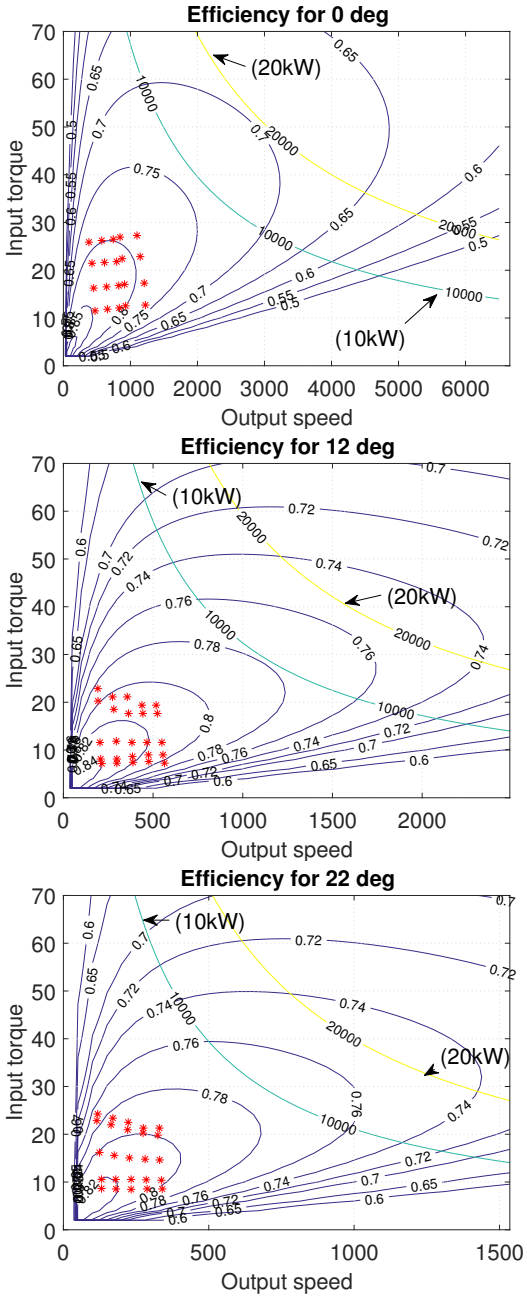

Fig. 17. Contours of mechanical efficiencies and locations of experimental data oints. Top: $i_{ideal} = 0.98$; Middle: $i_{ideal} = 2.61$; Bottom: $i_{ideal} = 4.23$. Note that some data points are hidden by the surfaces.

output shaft, operating at lower output speed (i.e. at higher ratios) even as the pump/motors are less efficient is beneficial.

V. Discussion

Experimental results confirm the general operation of the Hondamatic that when the motor displacement increases from 0 to the maximum, the transmission ratio increases from 1 to a maximum of 4.34 consistent with the estimated displacements of the pump and motor. As output load and speed increase, volumetric losses and mechanical losses accrue so that the input to output speed ratio increase and output to input torque ratio decrease.

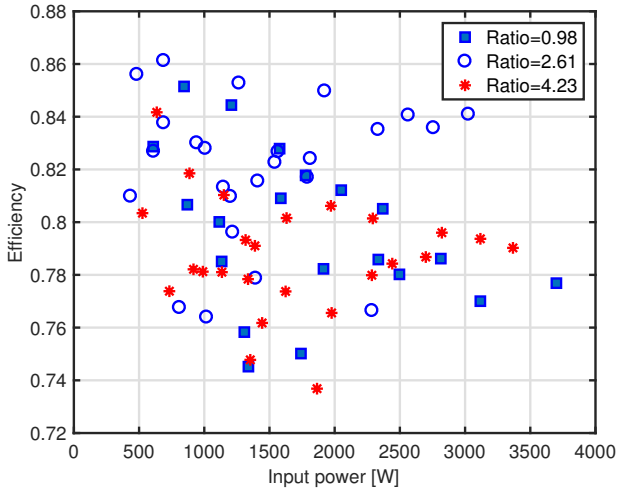

Fig. 18. Overall efficiencies versus input powers for different transmission ratios.

Study of the volumetric losses and volumetric efficiency show that leakage is small (since volumetric losses are small a speeds) but there are significant compressibility losses (that increase with pressure and speed). Volumetric losses are also the largest for $i_{ideal} = 0.98$ than at the other two ratios. The 3 paramters speed loss model in Section III-B is able to capture the speed loss characteristics at the three transmission ratios at which experiments were conducted. The model for the compressibility loss takes into account the variation of the motor dead volumes as displacement changes. Conceptually, the pump side and motor side compressibility loss coefficients should be related to the ratio of between the pump side and the motor side dead volumes according to $(s_{gm}(i_{max} - i_{ideal})/s_{gm})$. To see if this is true, consider the $i_{ideal} = 1$ case. The pump dead volume should be approximately the pump displacement, 6cc, (as the chamber is exposed to high pressure at the bottom dead center (BDC)). The motor dead volume should be approximately half of the maximum displacement, i.e. 18cc/2 = 9cc (as the pistons are stationary in the middle of the piston chamber). At this ratio, $(s_{gm}(i_{max} - i_{ideal})/s_{gm}0.0015 * (4.3 - 1)/0.0038 = 1.32$ which is similar to $9cc/6cc$. Both the experimental results and the model indicate that at $i_{ideal} = 0.98$, because the motor speeds are the highest (for a given range of input speeds) and the motor side dead volume is the largest (3.3 times and 1.7 times of volumes at the other ratios), the motor side compressibility loss is the greatest.

Analysis of the mechanical loss results indicates that there is significant no load viscous friction. The viscous coefficient is the largest at $i_{ideal} = 0.98$ and the lowest for $i_{ideal} = 2.61$. Mechanical loss increase with load at $i_{ideal} = 2.61, 4.23$ but not at $i_{ideal} = 0.98$. The 3-parameter (excluding stiction term) torque loss model in Section III-B and (32) is able to capture the torque loss characteristics at the three transmission ratios at which experiments were conducted. The model suggests that the motor side viscous damping coefficient is 4 times that on the pump side. This together with the fact that the motor

side friction is most strongly manifested at $i_{ideal} = 0.98$ are the reasons for the trend for the viscous coefficient. There are several possible reasons that the motor side viscous friction is so much larger than at the pump side. Firstly, the motor has 9 sets of pistons and distributor valves rather than 7 sets on the pump side. Since the structure of the pump and the motor are similar, this can likely contribute only 20% greater friction on the motor side than the pump side. Secondly and more probably, the motor rotation involves the rotation of both the pump and motor barrels that are immersed in a pool of oil which is not the case for the pump. The amount of oil in the test box is likely more than in an Hondamatic in normal operation. The churning of the oil may present significant extra viscous friction. Thirdly, the friction may be external to the Hondamatic such as due to the misaligment in the coupling between the output shaft and the load torque sensor. However, visual inspection does not reveal obvious misalignment.

Mechanical losses under loaded conditions include, in addition to the viscous friction present under no load condition, also a pressure dependent friction. The pressure dependent fiction is not significant for $i_{ideal} = 0.98$ case as predicted by model as there is little pumping or motoring. It contributes to approximately half and the majority of the mechanical losses at $i_{ideal} = 2.61$ and at $i_{ideal} = 2.61$ respectively. The pressure dependent friction is modeled to be proportional to pressure and to the pump and motor displacements. Since the pump displacement is constant, it is not possible to distinguish between displacement dependent and displacement independent friction. On the motor side, modeling only the displacement independent friction results in poor match of the mechanical losses, and modeling both the displacement dependent *and* independent friction results in a small coefficient for displacement independent friction and minimal improvement to the data fit. This suggests that motor side pressure dependent friction is dominated by displacement dependent friction. Physically, displacement dependent frictions are associated with the piston and piston bore interface, whereas displacement independent friction is associated with the piston shoe and swash plate interface and the barrel and valve plate interface. In the Hondamatic, the piston shoe and swash plate interface has been replaced by the rolling interfaces between the piston heads and the hemispheric indentations on the bearing supported shoe plate. Also, the valve plate has been replaced by the distributor valves. These design features are consistent with piston/bore friction dominating the pressure dependent friction. Although these observations are made for the motor side, because of the similar construction, it is also expected to be true of the pump side pressure dependent friction.

Analysis of the overall power loss and efficiency trends show that regular pressure independent friction and compressibility losses contribute most significantly to power loss. From Fig. 17, the overall efficiencies are relatively insensitive to output speed and input torque for all three transmission ratios. The ranges of efficiency observed at the three ratios tested are quite similar, although the intermediate ratio of 2.61 tends to be most efficient. Despite the fact that the experiments were conducted only at power below 3.5kW whereas the Hondamatic is intended for an engine with peak power of 20kW, the performance of the transmission can be evaluated at the higher power levels and at other ratios that are not tested by extrapolating the models (assuming they remain valid at these higher pressure and speeds). Fig. 17 shows that at the maximum engine power of 20kW, efficiencies at the 2.61 and 4.31 ratios are 75% whereas at the 0.98 ratio, it is 70%. Efficiency is over 70% for all feasiblle operating points (¡ 20kW, Tin¡60Nm, win¡6500rpm).

The premise of the Hondamatic as a hydromechanical transmission is that at $i_{ideal} \approx 1$, power is transmitted mechanically and so it was expected that transmission would be the most efficient at this ratio. It is therefore surprising that the efficiency at $i_{ideal} = 0.98$ is worse than that at the intemediate ratio of $i_{ideal} = 2.61$. By understanding how the various losses manifest themselves at various transmission ratios, we are able to attribute the relatively poor performance to motor side viscous friction and compressibility losses. Specifically, the viscous friction on the motor or output side is 4 times that on the pump side, and that because of dead volume in the motor is the largest at $i_{ideal} \approx 1$, the compressibility loss is worst at this ratio. By specifically addressing these losses, the performance at $i_{ideal} \approx 1$ can be improved. Since compressibility losses is primarily an issue with valve timing, it may be addressed by redesigning the distributor valve to incorporate pre-compression and de-compression. In the case of $i_{ideal} = 1$ when the motor pistons are stationary, locking up the valve completely can be an option. If the large motor side no-load viscous friction observed above is indeed contributed by churning losses due to excessive oil in the test box or by misalignment, part of this viscous friction can be reduced. Suppose that half of the motor side viscous friction is compensated (i.e. $b_m = 0.0018 \rightarrow 0.0009$Nm/rpm), it can be shown that the mechanical efficiencies at the 0.98 ratio are substantially improved by 1-8%, whereas at the 2.61 and 4.23 ratios, the mechanical efficiencies are only improved by less than 2.5% and 0.8% respectively. The difference in levels of improvement is because the effect of motor side friction is most dominant when $i_{ideal} \approx 1$ and less for larger i_{ideal} and that at the larger ratios, the motor speeds are much lower in the tests. The effect of compensating for the motor side viscous friction is that the overall efficiency at the 0.98 ratio is improved by 1-7.3%, at the 2.61 ratio by 0.2-2.2% and at the 4.23 ratio by 0.08-0.67% (Fig. 19).

Finally, by combining an average model that consider different types of mechanical and volumetric losses and experiment testing, we are able to estimate the what the dominant losses are within the Hondamatic. These findings can be further validated by developing a detailed model of the Hondamatic that explicitly models the physical loss phenomena, such as different leakages and frictions at different interfaces. This work is in progress and will be presented in a future paper.

VI. Conclusions

In this paper, a highly compact hydro-mechanical transmission - the Hondamatic, has been analyzed via a combination of modeling and experimentation. The Hondamatic achieves

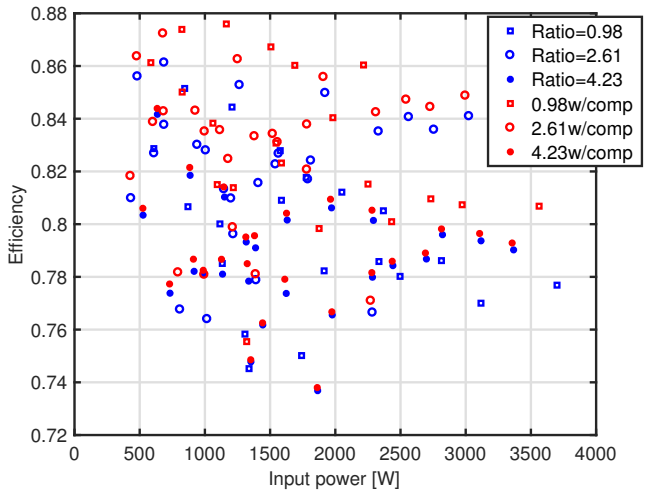

Fig. 19. Overall efficiencies versus input powers for different transmission ratios with viscous friction compensated

its compactness by subsuming the function of the planetary gear set with a two-shafted pump so that the rotation of the piston barrels of the pump and the motor can be dual-used for transmitting mechanically. By using a distributor valve mechanism instead of valve plates, friction and leakage normally associated valve plates are avoided. An average model has been developed that reveals the operating principle and how different component level mechanical and volumetric losses manifest themselves at different transmission ratios. Using experimental performance at three transmission ratios, the average model with losses is fitted with only seven empirical parameters to describe the volumetric and mechanical losses. The resulting model can be used to extrapolate the performances at all ratios and operating conditions. Efficiency is not the highest when the transmission ratio is near unity and rotates as a rigid body, as originally expected. The reason is that the unit tested has significant no-load viscous friction and compressibility losses, especially on the motor side, which are more dominant at the unity ratio. Despite these losses, the overall efficiency is above 70% in most working conditions. By further identifying and addressing the source of the motor side viscous friction and reducing compressibility losses, the Hondamatic would be even more efficient and versatile.

ACKNOWLEDGMENT

This work was performed during the visits by the first (X. Hu) and second (C.B. Jing) authors to the Center for Compact and Efficient Fluid Power (CCEFP), supported by the National Science Foundation (EEC-0540834), at the University of Minnesota. Travel and stipend support provided by the China Scholarship Council to X. Hu and C. Jing was gratefully acknowledged.

REFERENCES

[1] J. H. Kress, “Hydrostatic power splitting transmissions for wheeled vehicles classification and theory of operation”. SAE paper 680549, Society of Automotive Engineers, Warrendale, PA, 1968.

[2] F. Jarchow, Leistungsverzweigte Getriebe (Power split transmissions), VDI-Z. 106 (6) (1964) 196205.

[3] T. Kohmscher, Modelbildung, Analyse und Auslegung hydrostatischer Antriebsstrangkonzepte, Ph.D. dissertation, RWTH Aachen, Germany, 2008.

[4] B. Carl, M. Ivantysynova, and K. Williams. “Comparison of Operational Characteristics in Power Split Continuously Variable Transmissions”, SAE Technical Paper, 2006-01-3468, 2006.

[5] M. Alarico, and A. Rossetti. “Optimization of hydro-mechanical power split transmissions.” Mechanism and Machine Theory 46.12(2011):1901-1919.

[6] Z. Du, K. L. Cheong, P. Y. Li and T. R. Chase, “Fuel Economy Comparisons of Series, Parallel and HMT Hydraulic Hybrid Architectures”, 2013 American Control Conference, Washington D.C., June 2013.

[7] D. Sung, S. Hwang and H. Kim, “Design of hydromechanical transmission using network analysis”, Proceedings of the Institution of Mechanical Engineers, Part D: Journal of Automobile Engineering, Vol. 210(1), 2005. pp. 53-63.

[8] K. Pettersson and P. Krus, “Design optimization of complex hydromechanical transmission”, Journal of Mechanical Design, Vol. 135/091005-1, 2013.

[9] A. Rossetti, A. Macor and M. Scamperle, “Optimization of components and layouts of hydromechanical transmissions”, International Journal of Fluid Power, 18:2, 2017, pp. 123-134.

[10] K. L. Cheong, P. Y. Li and T. R. Chase, “Optimal Design of Power-Split Transmission for Hydraulic Hybrid Passenger Vehicles”, 2011 American Control Conference, pp.3295-3300, San Francisco, CA, June, 2011.

[11] L. H. Reimer, “Neutral Control for Hydraulic Transmission”, U.S. Patent 3,698,189, October 17, 1972.

[12] Honda. ”Hondamatic-Hydraulic Mechanical Transmission”, http://world.honda.com/motorcycle-technology/Hondamatic/

[13] M. Saitou, H. Okuzaki, T. Kazuhiro and S. Takeuchi, “Hydraulic Continuously Variable Transmission”, U.S. Patent 7,000,388 B2, February, 21, 2006.

[14] Honda. “Brochure of FourTrax Foreman Rubicon, http://powersports.honda.com/2014/fourtrax-foreman-rubicon.aspx, 2014.

[15] T. J. Cyders, “Analysis and Experimental Comparison of Models of a New Form of Continuously Variable Transmission,” Doctoral dissertation, Department of Mechanical Engineering, Ohio University, 2012.